Analyses of the Northern European Summer Heatwave of 2018

Pascal Yiou, Julien Cattiaux, Davide Faranda, Nikolay Kadygrov, Aglaé Jézéquel, Philippe Naveau, Aurélien Ribes, Yoann Robin, Soulivanh Thao, Geert Jan J van Oldenborgh, et al.

Analyses of the European summer heatwave of 2018

P. Yiou (1), J. Cattiaux (2), D. Faranda (1,3), N. Kadygrov (1), A. Jézéquel (4,6), P. Naveau (1), A. Ribes (2), Y. Robin (2), S. Thao (1), G.J. van Oldenborgh (5), M. Vrac (1)

(1) Laboratoire des Sciences du Climat et de l'Environnement, UMR8212 CEA-CNRS-UVSQ, IPSL and U Paris Saclay, Gif-sur-Yvette, France.
(2) Centre National de la Recherche en Météorologie, UMR CNRS-Météo France, Toulouse, France
(3) London Mathematical Laboratory, London, UK
(4) Laboratoire de Météorologie Dynamique, UMR CNRS-ENS-UPMC-X, Paris, France
(5) KNMI, De Bilt, Netherlands
(6) Ecole Nationale des Ponts et Chaussées, Champs-sur-Marne, France

Capsule

A heatwave struck northern Europe in summer 2018. The probability of this event increased with human-induced climate change. The properties of the atmospheric circulation are not deemed to change.

Introduction

A heatwave struck northern Europe in the summer of 2018. Daily temperature anomalies reached 14K in Scandinavia, the Netherlands and Belgium, where records of temperature were broken. This heatwave was exacerbated by a drought caused by the same circulation anomaly. The heatwave and drought favored unprecedented forest fires in Scandinavia.
This paper aims at characterizing this heatwave event and determining its probability in present and future climate conditions. Special issues of the BAMS have shown a large variety of statistical approaches to event attribution (Jézéquel et al. 2018b). Such approaches can provide contrasting results and interpretations, depending on hypotheses, some of which can be very technical and/or subtle. This paper presents how the 2018 heatwave can be analysed in terms of temperature and atmospheric circulation patterns, and highlights potential quantitative discrepancies that are due to statistical hypotheses.

Defining the event

Defining the spatio-temporal scale of the event is inspired by the procedure of (Cattiaux and Ribes 2018), which consists in selecting the space-time window for which the temperature has been the most extreme (i.e. its probability is the smallest in present-day conditions). We use E-OBS (Haylock et al. 2008) daily mean temperatures over 1950-2018 and consider

each N-day time window between May 1 and October 31, and each n-country connected spatial domain.Overall, we find that p is minimum for the 19-day window between July 15 - August 2 and the 2-country domain covering Finland - Sweden. However this minimum is not sharp and adding Baltic countries, Denmark and Norway to the spatial domain does not significantly change p. Since a larger domain is more suitable for the rest of the analyses, we define the spatial scale as the 5-30°E, 55-70°N area (Fig. 1a). This corresponds to the "Scandinavian cluster" type of heatwave identified by (Stefanon et al. 2012). Over this space-time window, the temperature anomaly relative to 1981-2010 is 5.4 K (Fig. 1c), and each single day is more than 3K above the seasonal cycle for 2018 (Fig. 1d). The atmospheric circulation is characterized by prolonged high pressure conditions (Fig. 1b) over Scandinavia. This motivates the conditional attribution analysis (with respect to the atmospheric circulation), because such circulation patterns generally enhance major heatwaves (Quesada et al. 2012; Mueller and Seneviratne 2012), as was observed in summers 2003 (Schaer et al. 2004) or 2010 (Barriopedro et al. 2011).

Unconditional attribution

The unconditional attribution compares the probability p1 of observing the event (of exceeding a temperature threshold) in present day or in a climate influenced by humans (a factual world), and the probability p0 of the event in past conditions or in a climate without human influence (a counterfactual world). We focus on the risk ratio (RR) p1/p0. The results from two different approaches are presented here.

First, a nonstationary estimate of probabilities was performed on the E-OBS dataset and a CMIP5 (Taylor et al. 2012) simulation ensemble using the method of (Ribes et al.). The distribution of mean temperature over the considered space-time domain is assumed to follow a Gaussian distribution, and to covary with a variable representing climate change. We use the summer mean continental temperature over the box -10E-30Ex35N-70N as a covariate. The probability of the event can be estimated continously in time. This calculation is (i) made for each CMIP5 model, (ii) summarized into a multimodel synthesis, and (iii) combined with E-OBS observations, as presented in (Ribes et al.). Fig. 2a. shows the risk ratio from 1850 to 2100, under the RCP8.5 scenario, according to the multimodel synthesis constrained by observations. The effect of human activities on the probability of such event cannot be detected before the end of 20th century as the risk ratio is not significantly different from 1. After the year 2000, the risk ratio is significantly higher than 1 and suggests that human activities have increased the risk ratio of such events. In 2018, the probability of such events has increased by a factor of 39 (95% confidence interval: 3 -- 3400) due to human activity.

Second, we determined p1 and p0 from annual maximum 19-day averaged temperature over the region in E-OBS data by fitting the period 1950-2017 to a generalized extreme value (GEV) distribution where the location parameter μ is a linear function of a proxy for global warming, for which we take the 4-yr smoothed global mean surface temperature (as in (Kew et al. 2019)). This procedure differs from the preceding one on the probability distribution choice: the trend is estimated from the observations rather than CMIP5 and it excludes the observed extreme in 2018, as GEV parameter estimates are sensitive to the last value of a time series. This procedure was repeated for a few large ensembles of transient climate model experiments with realistic variability of 19-day heat extremes. We plot the risk ratios (RR=p0/p1) in Fig. 2b. The white boxes represent the model spread that is

added to the coloured boxes representing uncertainty due to natural variability to obtain χ^2/dof=1. This diagnostic shows that the risk ratio is significantly larger than 1, with a large range of variations (RR between 5 and 2000).

Conditional attribution

We assess the temperature distribution conditional to atmospheric patterns that are similar to 2018 changes with time. Following the procedure of (Jézéquel et al. 2018c), we computed analogues of Z500 over a zone covering Scandinavia (rectangle in Fig. 1b), which optimizes the temperature/circulation correspondence. The analogues are computed from Z500 in two subperiods (1950-1984; 1985-2018) of the NCEP reanalysis (Kistler et al. 2001). The Z500 data are detrended with a smoothing spline before computing analogues, in order to avoid a bias due to the temperature increase. Mean analogue temperatures are simulated by random selections of analogue days from each subperiod, following the procedure of (Jézéquel et al. 2018c). The change of temperature probability distributions describes the thermodynamic changes on a summer that is similar to 2018. 10000 stochastic samples are generated, with analogues selected in the two subperiods.

Although the simulated values do not reach the 2018 record, we find a significant increase of the temperature distribution between the two subperiods (Fig. 2c). This ~1K increase is comparable to the average increase of temperature between the two subperiods. When analogues are selected in RCP8.5 CMIP5 simulations, we find that similar atmospheric patterns lead to summer temperatures that are consistent with the 2018 record values. This means that temperature anomalies of a similar heatwave (same domain, duration, and atmospheric circulation) would reach or exceed 5K by the end of the 21st century.

Changes in atmospheric circulation

We diagnosed atmospheric circulation trends by analysing the distance values of the best analogues (Jézéquel et al. 2018a), the local dimension and persistence (Faranda et al. 2017). This was done by comparing the observed Z500 anomaly sequence (in NCEP), and other observed sequences in NCEP or simulated in RCP 4.5 and 8.5 scenarios.

First, we computed the distribution of Z500 distances to the hottest day of the heatwave (17th July 2018) in NCEP and RCP 4.5 and 8.5 scenario simulations. We then counted the number of analogues whose distance is below the 5th quantile of all distances, for each summer. The distance distribution informs on the likelihood to have a similar atmospheric pattern as the observed one (Jézéquel et al. 2018a). We find no significant trend in the number of good analogues in NCEP reanalysis or scenario simulations (Fig. S1b): some CMIP5 simulations do identify marginally significant trends, but there is no consensus among models, as was found for the 2003 heatwave (Jézéquel et al. 2018a).

Second, we computed the local dimension of the observed Z500 sequence in CMIP5 RCP simulations. This assumes that the observed state belongs to the climate attractor described by climate models, which is validated by the fact that the distribution of analogue distances for each model is similar to the NCEP reanalysis distances (Rodrigues et al. 2018). The local dimension informs on the number of degrees of freedom of trajectories around a given state and hence on its predictability (Faranda et al. 2017). We find no significant trend in the local dimension of summer 2018 Z500 in CMIP5 RCP simulations.

Third, the extremal index informs on the persistence of a given state, i.e. the time it takes to

leave its neighborhood in phase space. As for the local dimension, the local persistence of summer 2018 Z500 was evaluated on CMIP5 RCP simulations. We find a small but significant decrease of the persistence of those weather patterns (Fig. 2f).

Conclusions

Those analyses demonstrate the thermodynamic contribution of human-induced climate change to describe the probability and intensity of the summer 2018 event in Scandinavia. The bulk values of the risk ratios are similar and significantly larger than 1 in the two approaches. We also find that the range of uncertainties are similar, although underlying technical assumptions differ.

The atmospheric conditions enhance the temperature signal (~2K), but the conditional attribution simulations cannot reach the observed record values, because some physical processes are not taken into account (soil moisture and ocean variability).
Those results emphasize the interest of systematic analyses of European heatwaves (Stefanon et al. 2012), for which the properties of the atmospheric circulation do not change uniformly in scenario simulations (Jézéquel et al. 2018a).

Acknowledgements

This paper was supported by EUPHEME project, which is part of ERA4CS, an ERA-NET initiated by JPI Climate and co-funded by the European Union (Grant #690462), ERC grant no. 338965-A2C2, and French “Convention de Service Climatique”. The analyses of this paper were obtained with the Climate Explorer (https://climexp.knmi.nl/start.cgi) and the “blackswan” Web Processing Service (https://github.com/bird-house/blackswan).

References

Barriopedro, D., E. M. Fischer, J. Luterbacher, R. M. Trigo, and R. García-Herrera, 2011: The hot summer of 2010: redrawing the temperature record map of Europe. *Science*, **332**, 220–224.

Cattiaux, J., and A. Ribes, 2018: Defining single extreme weather events in a climate perspective. *Bulletin of the American Meteorological Society*,.

Faranda, D., G. Messori, and P. Yiou, 2017: Dynamical proxies of North Atlantic predictability and extremes. *Scientific reports*, **7**, 41278.

Haylock, M. R., N. Hofstra, A. M. G. K. Tank, E. J. Klok, P. D. Jones, and M. New, 2008: A European daily high-resolution gridded data set of surface temperature and precipitation for 1950-2006. *J. Geophys. Res. - Atmospheres*, **113**, doi:10.1029/2008JD010201.

Jézéquel, A., J. Cattiaux, P. Naveau, S. Radanovics, A. Ribes, R. Vautard, M. Vrac, and P. Yiou, 2018a: Trends of atmospheric circulation during singular hot days in Europe. *Environmental Research Letters*, **13**, 054007.

——, V. Dépoues, H. Guillemot, M. Trolliet, J.-P. Vanderlinden, and P. Yiou, 2018b: Behind the veil of extreme event attribution. *Climatic Change*,

https://doi-org.insu.bib.cnrs.fr/10.1007/s10584-018-2252-9. https://doi.org/10.1007/s10584-018-2252-9.

——, P. Yiou, and S. Radanovics, 2018c: Role of circulation in European heatwaves using flow analogues. *Climate Dynamics*, **50**, 1145–1159.

Kew, S. f, S. Y. Philip, G. Jan van Oldenborgh, G. van der Schrier, F. E. Otto, and R. Vautard, 2019: The Exceptional Summer Heat Wave in Southern Europe 2017. *Bulletin of the American Meteorological Society*, **100**, S49–S53.

Kistler, R., and Coauthors, 2001: The NCEP-NCAR 50-year reanalysis: Monthly means CD-ROM and documentation. *Bulletin of the American Meteorological Society*, **82**, 247–267.

Mueller, B., and S. I. Seneviratne, 2012: Hot days induced by precipitation deficits at the global scale. *Proc. Natl. Acad. Sci. USA*, doi:10.1073/pnas.1204330109, https://doi.org/10.1073/pnas.1204330109.

Naveau, P., A. Ribes, F. Zwiers, A. Hannart, A. Tuel, and P. Yiou, 2018: Revising return periods for record events in a climate event attribution context. *Journal of Climate*, **31**, 3411–3422.

Quesada, B., R. Vautard, P. Yiou, M. Hirschi, and S. I. Seneviratne, 2012: Asymmetric European summer heat predictability from wet and dry southern winters and springs. *Nature Climate Change*, **2**, 736–741, https://doi.org/Doi 10.1038/Nclimate1536.

Ribes, A., S. Thao, and J. Cattiaux, Describing the relationship between a weather event and climate change: a new statistical approach. *submitted to J. Clim.*, https://hal.archives-ouvertes.fr/hal-02122780/document.

Rodrigues, D., M. C. Alvarez-Castro, G. Messori, P. Yiou, Y. Robin, and D. Faranda, 2018: Dynamical properties of the North Atlantic atmospheric circulation in the past 150 years in CMIP5 models and the 20CRv2c Reanalysis. *Journal of Climate*,.

Schaer, C., P. Vidale, D. Luthi, C. Frei, C. Haberli, M. Liniger, and C. Appenzeller, 2004: The role of increasing temperature variability in European summer heatwaves. *Nature*, **427**, 332–336.

Stefanon, M., F. D'Andrea, and P. Drobinski, 2012: Heatwave classification over Europe and the Mediterranean region. *Environmental Research Letters*, **7**, 014023.

Taylor, K. E., R. J. Stouffer, and G. A. Meehl, 2012: An Overview of CMIP5 and the Experiment Design. *Bull. Amer. Met. Soc.*, **93**, 485–498.

Figures

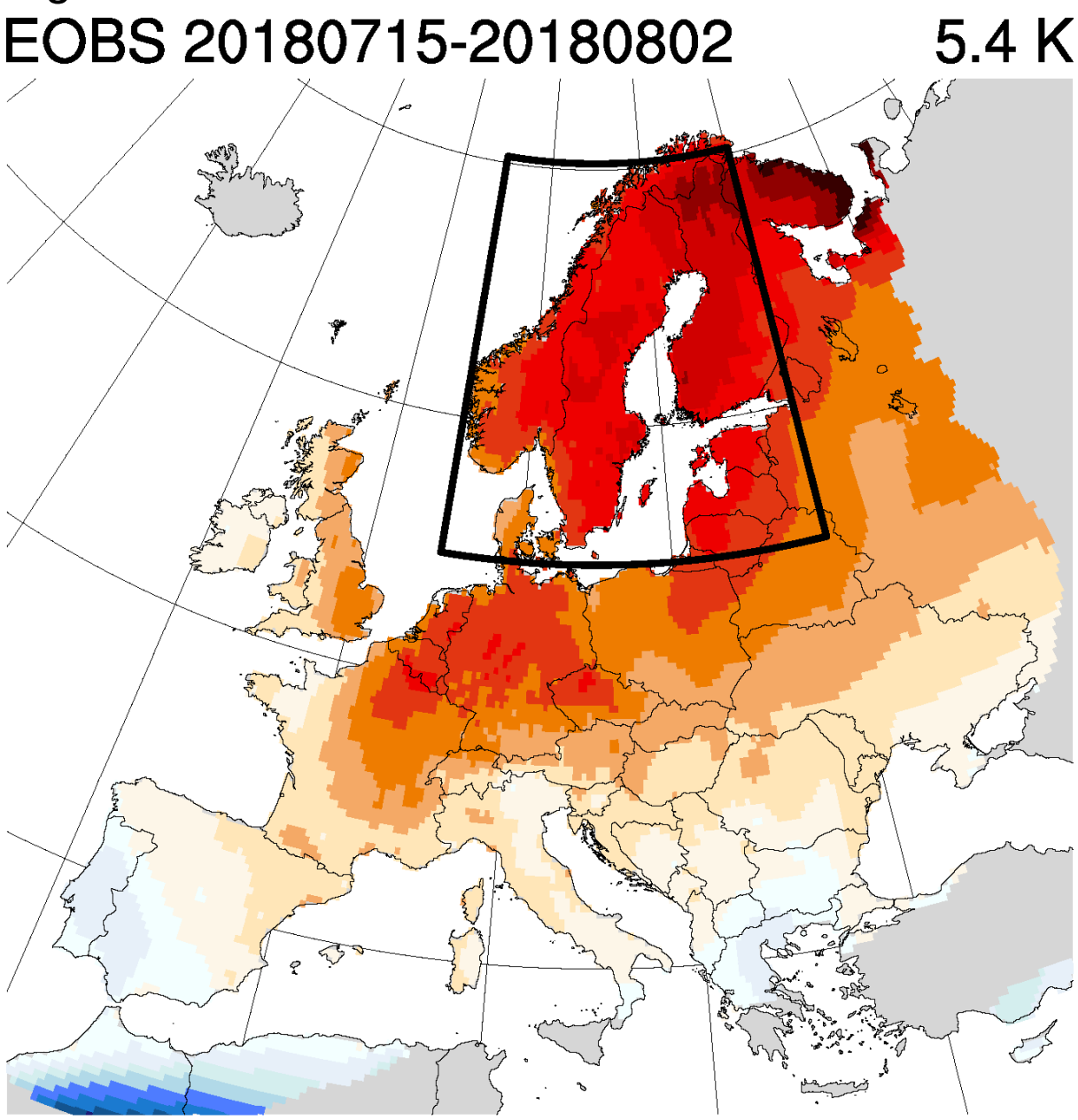
EOBS 20180715-20180802
5.4 K
T anomaly wrt. 1981-2010 (K)
-8 -7 -6 -5 -4 -3 -2 -1 0 1 2 3 4 5 6 7 8

a

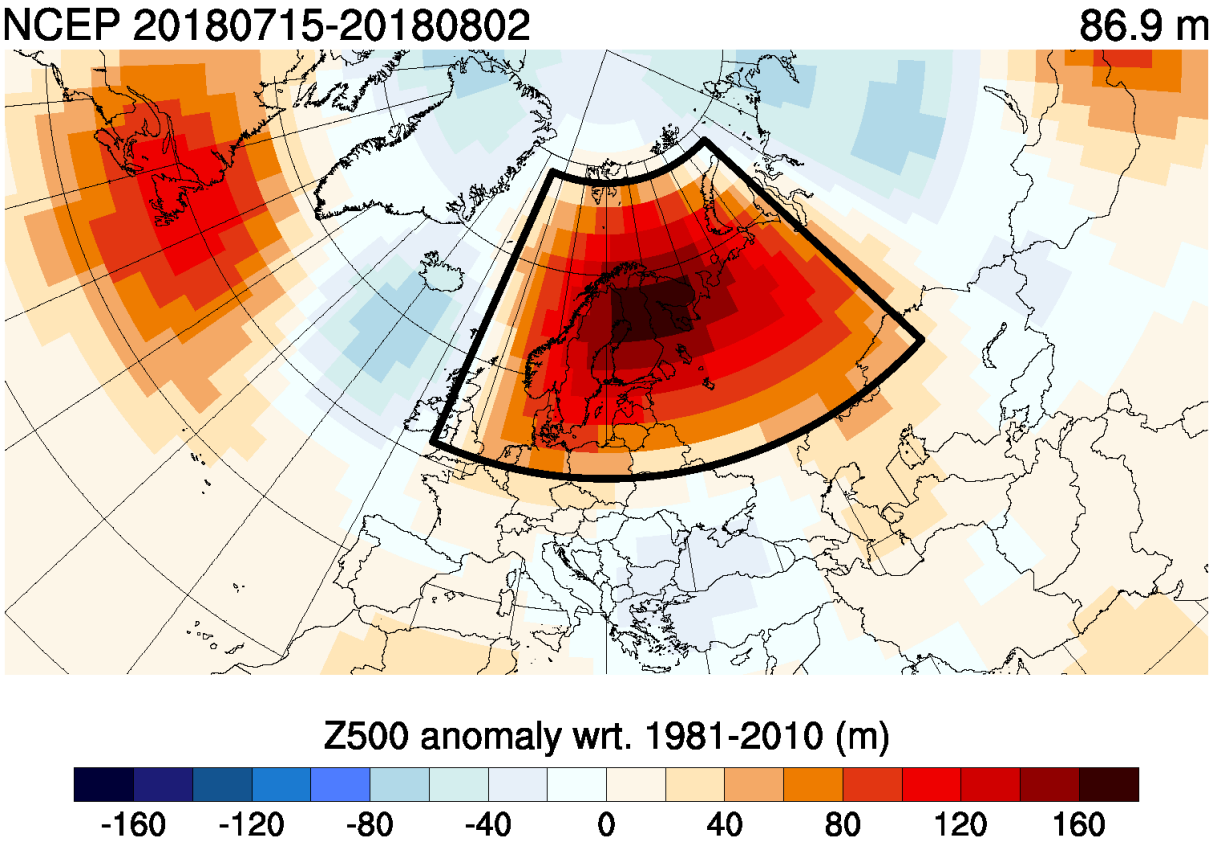
NCEP 20180715-20180802
86.9 m
Z500 anomaly wrt. 1981-2010 (m)
-160
-120
-80
-40
0
40
80
120
160

b

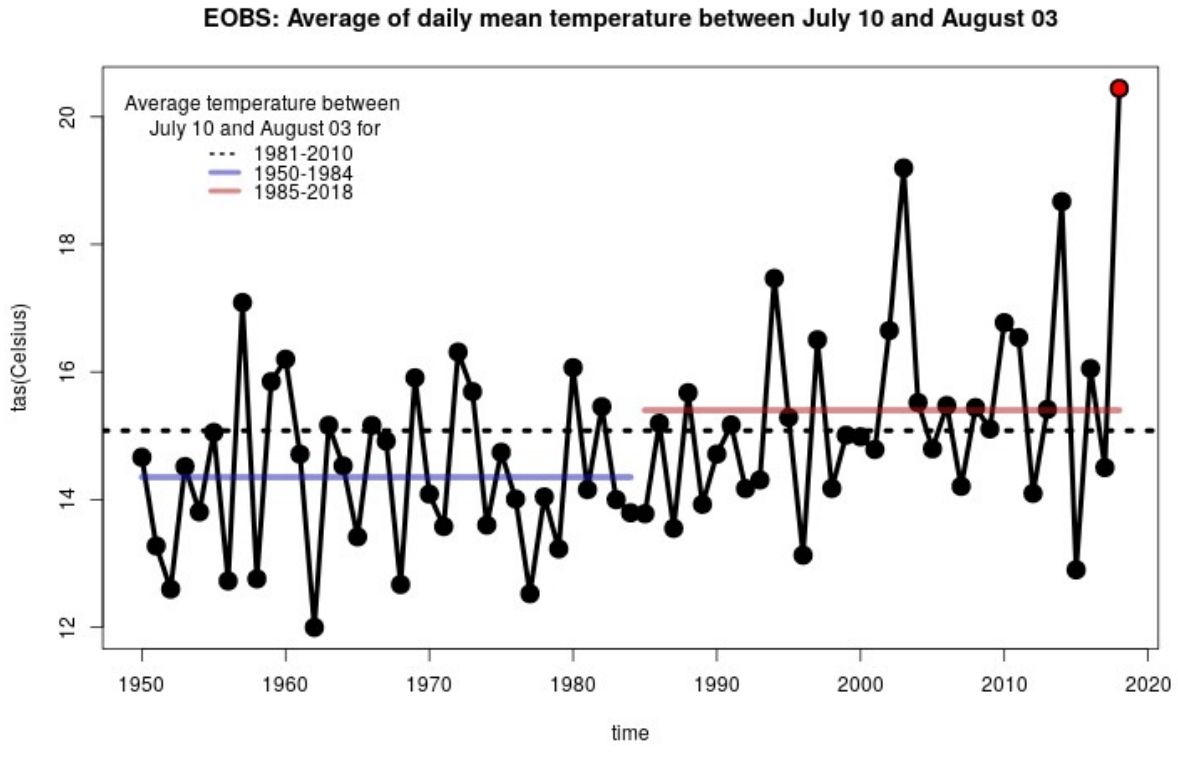
EOBS: Average of daily mean temperature between July 10 and August 03
Average temperature between
July 10 and August 03 for
1981-2010
1950-1984
1985-2018
tas(Celsius)
12
14
16
18
20
1950
1960
1970
1980
1990
2000
2010
2020
time

c

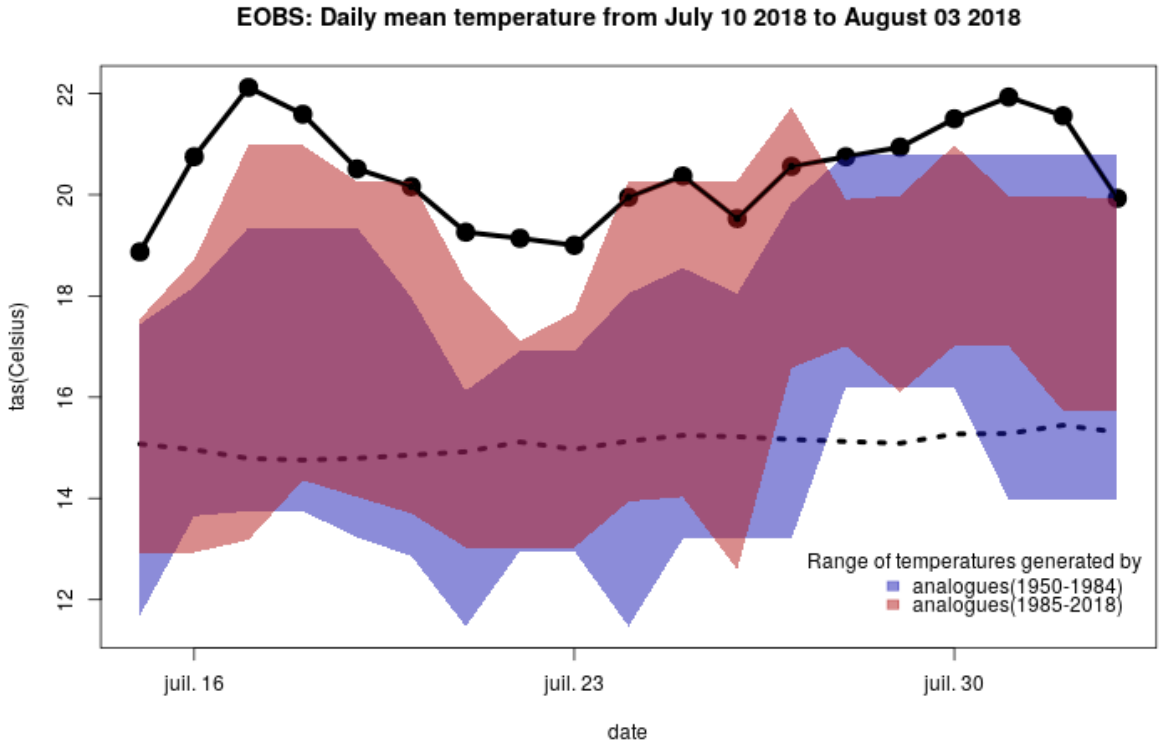

d

Figure 1: Geographical and temporal features of the event from reanalyses & observations. Panel a. Map of Temperature Anomalies in EOBS between July 15th 2018 and August 2nd 2018. The rectangle indicates the zone to be analyzed (e.g. Scandinavia). Panel b. Anomalies of Z500 in NCEP over the North Atlantic between July 15th 2018 and August 2nd 2018. The rectangle indicates the zone for the computation of analogues. Panel c. Time series of spatial (rectangle in a) & temporal (15 July to 2 August) average temperature (EOBS) from 1950 to 2018, with reference climatology. Panel d. Time series of daily temperature from 15 July to 2 August 2018 (continuous line), with a plot of the seasonal cycle (dotted line). The shaded areas indicate the range of daily variations of analogue temperatures.

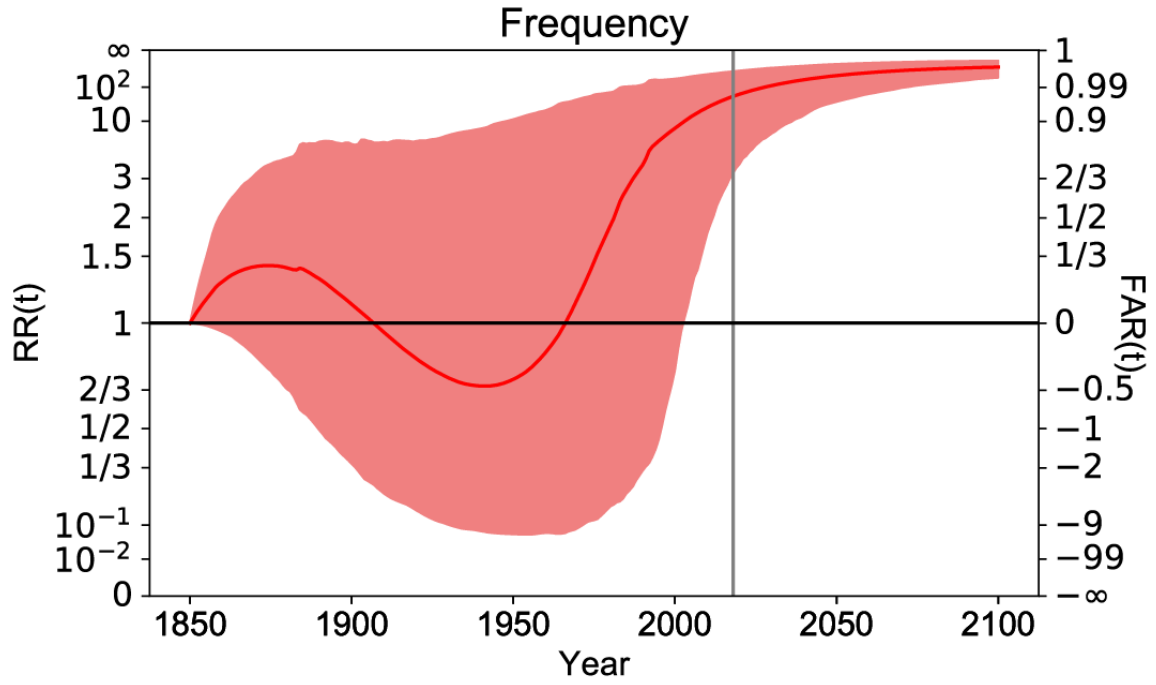
Frequency
RR(t)
FAR(t)
Year
∞
10²
10
3
2
1.5
1
2/3
1/2
1/3
10⁻¹
10⁻²
0
1
0.99
0.9
2/3
1/2
1/3
0
−0.5
−1
−2
−9
−99
−∞
1850
1900
1950
2000
2050
2100

a

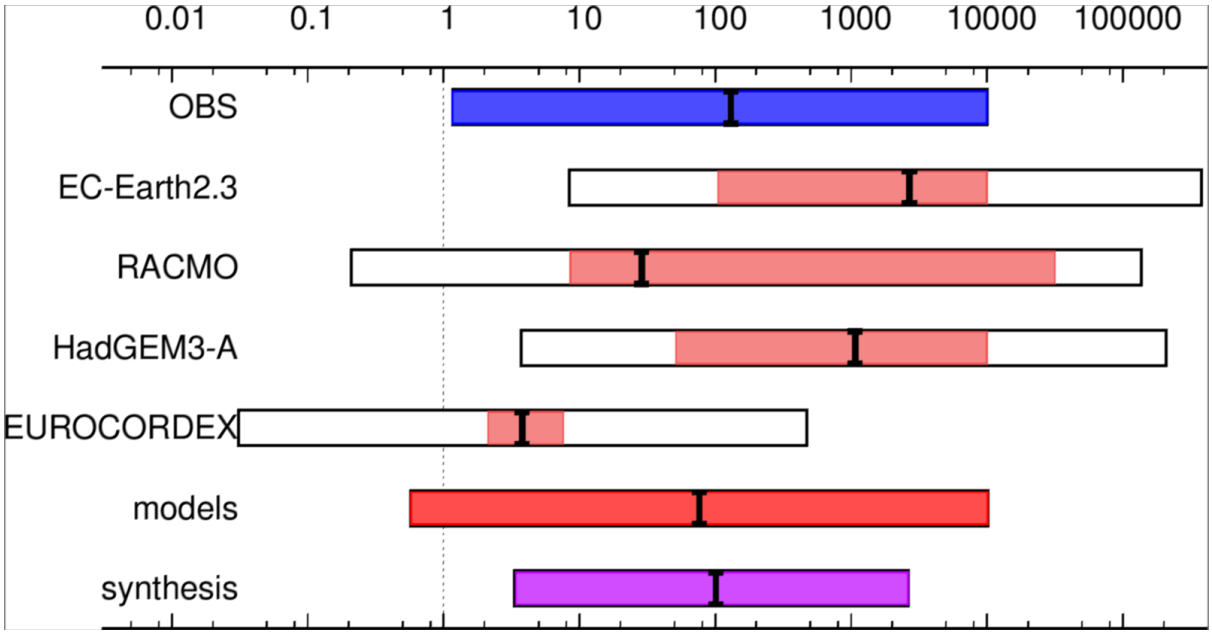
0.01
0.1
1
10
100
1000
10000
100000
OBS
EC-Earth2.3
RACMO
HadGEM3-A
EUROCORDEX
models
synthesis

b

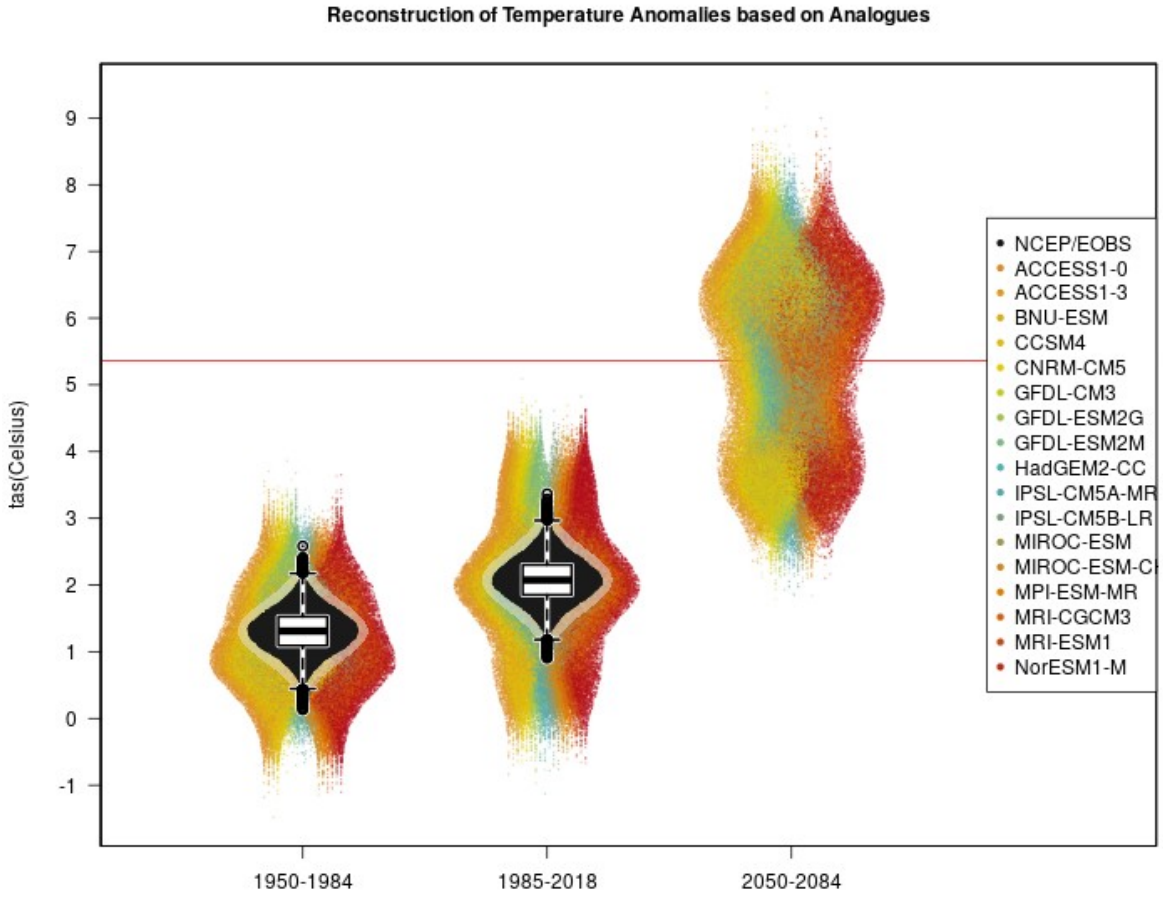

c

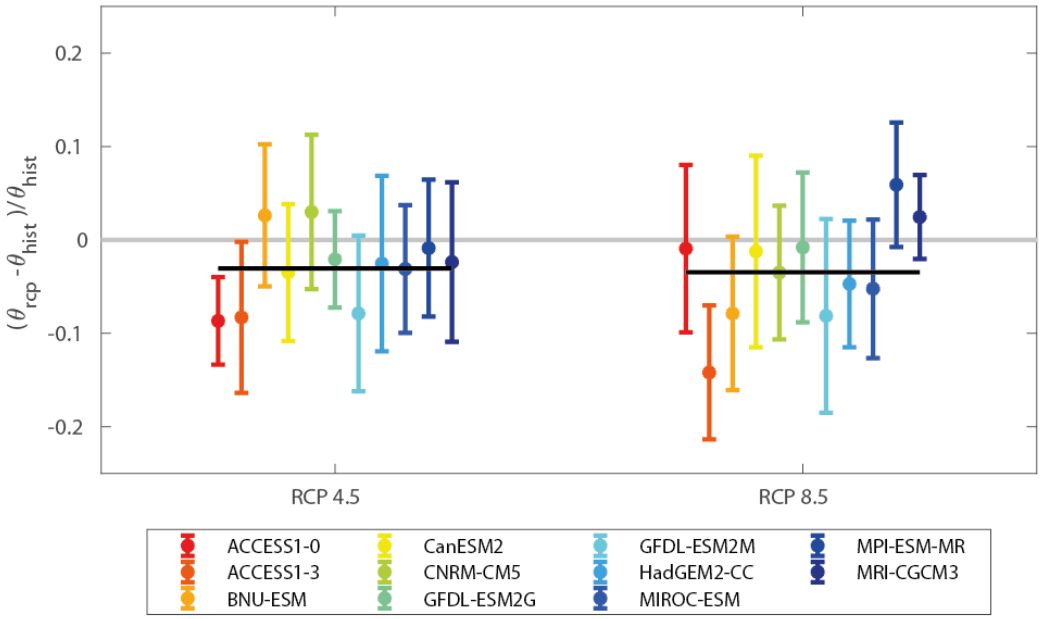

f

Figure 2. Panel a: Unconditional attribution (RR) from CMIP, i.e. one of the panels below. The red continuous line is the best estimate for the risk ratio (RR), and the red zone is the

confidence interval at level 95%. The vertical grey line is the date of the event (2018). The red shaded area represents the confidence interval at the 95% level, computed by a bootstrap procedure (1000 samples). **Panel b.** Risk ratios (RR) from observations (EOBS), and climate model simulations (EC-EARTH, RACMO, HadGEM3, Euro-CORDEX ensemble), all models, and observation-model synthesis. **Panel c**. Conditional temperature simulations in CMIP5. Each point denotes one temperature value generated with the analogues for the same period. Black points, temperature generated from NCEP/EOBS. Coloured points, temperature generated by GCMs. The boxplot show the quartiles of the temperatures generated from NCEP/EOBS. The red line denotes the value of the observed mean temperature between July 15 and August 2 2018. **Panel f**. Relative changes in the persistence of the Z500 atmospheric circulation associated to 2018 heatwave. Each bar represents the median and the standard deviation of the persistence over the period for each CMIP5 model used. The black horizontal line represent the multimodel mean.